

# Supernova Remnants and Plerions in the Compton Gamma-Ray Observatory Era

Ocker C. de Jager\* and Matthew G. Baring,<sup>†1</sup>

\*Space Research Unit, PU vir CHO, Potchefstroom 2520, South Africa

<sup>†</sup>Laboratory for High Energy Astrophysics, Code 661,  
NASA Goddard Space Flight Center, Greenbelt, MD 20771, USA

**Abstract.** Due to observations made by the Compton Gamma-Ray Observatory over the last six years, it appears that a number of galactic supernova remnants may be candidates for sources of cosmic gamma-rays. These include shell-type remnants such as IC443 and  $\gamma$  Cygni, which have no known parent pulsars, but have significant associations with unidentified EGRET sources, and others that appear to be composite, where a pulsar is embedded in a shell (e.g. W44 and Vela), or are purely pulsar-driven, such as the Crab Nebula. This review discusses our present understanding of gamma-ray production in plerionic and non-plerionic supernova remnants, and explores the relationship between such emission and that in other wavebands. Focuses include models of the Crab and Vela nebulae, the composite nature of W44, the relationship of shell-type remnants to cosmic ray production, the relative importance of shock-accelerated protons and electrons, constraints on models placed by TeV, X-ray and radio observations, and the role of electrons injected directly into the remnants by parent pulsars. It appears as if *relic electrons* may be very important in the Vela and Crab remnants. The recent observation of the TeV hot spot in the Vela remnant, which is offset from the current pulsar position, is attributed to relic electrons that were left at the birthplace of the pulsar, the offset being due to the proper motion of the Vela pulsar during its 11,000 year lifetime. We also discuss the role of *freshly-injected* electrons in the remnants around the Crab, Vela and PSR B1706-44 pulsars. These electrons can acquire energies that tap up to at least 10 percent of the full pulsar polar potential, and can produce prominent synchrotron and inverse Compton radiation signatures. The various recent models for predicting gamma-ray emission in shell-type remnants are summarized. The constraining upper limits to TeV emission from such remnants obtained by the Whipple Observatory indicate that either the emission due to particles accelerated at remnant shocks is too faint to be detected by EGRET, or that conditions near their shells (e.g. high density, low magnetic field) limit the acceleration of particles to below a few TeV.

---

<sup>1</sup>) Compton Fellow, Universities Space Research Association

## PULSAR-DRIVEN NEBULAE (PLERIONS).

A number of plerions have been discovered in radio, optical, and X-rays [71], with the Crab as the youngest and most energetic source. Plerionic nature is usually indicated by a center-filled morphology, resulting from the continuous injection of pulsar electrons into the nebula, with the additional constraint that the spectra must be non-thermal (power-law) resulting from a statistical acceleration processes. The reason for the latter constraint is that some center-filled X-ray remnants show evidence for thermal emission such as W44 [48], resulting from the presence of hot gas from the central regions.

The radio, optical and X-ray emission observed in plerions is believed to be due to synchrotron emission. Observations map the product of the field strength (to some power) and the number of energetic particles via the synchrotron brightness, however the spectral components from different wavebands cannot be separated unless another emission mechanism is observed from the same particle population. An example of this is inverse Compton scattering, where the magnetic field is replaced with a photon density as a “target” for the high energy particles, and observations of both processes lead to a determination of the field strength. Inverse Compton emission is usually seen at higher energies compared to synchrotron emission, and a multiwavelength study of a source allows us to simultaneously probe the synchrotron and inverse Compton processes, thereby permitting measurement of both the magnetic field strength and the total energy budget of the electrons. In fact, Compton Gamma-Ray Observatory (CGRO) observations of the Crab Nebula provided the first detection of the transition from synchrotron to inverse Compton emission [19], whereas CGRO observations of the Vela remnant are limited to the OSSE instrument (see Fig. 2), and therefore allow us to probe only the synchrotron component of the Vela spectrum.

### Constraints on the development of a plerion

The first condition for the development of a synchrotron nebula around a pulsar is that some fraction of the Poynting flux from the pulsar should be transferred to electrons. This means that the ratio  $\sigma$  of Poynting to particle energy fluxes should not be too large. The second condition is that either a shock (at an angular distance  $r_s$ ), or an instability in the wind (at an angular distance  $r_o$ ) should remove the electrons from the comoving frame of the pulsar wind, so that the electrons can “see” an effective perpendicular field component for synchrotron radiation [51]. For example, high resolution HST images of the Crab pulsar/nebula shows that the first knots (disturbances in the relativistic unperturbed flow) are seen at a distance of  $r_o < 1''$  on its polar axis [43], whereas the pulsar wind shock is expected at  $r_s \sim 8'' - 10''$  [51]. The

combination of these two effects (energy transfer and the “visibility” of a field for synchrotron radiation) results in plerionic synchrotron emission outside a minimum distance from the pulsar. The development of a shock also allows the pulsar wind to be slowed down from relativistic speeds to the speeds of typical expanding supernova ejecta.

## The Crab Nebula

The Crab Nebula is the prototype cosmic source of synchrotron radiation and inverse Compton (IC) scattering [39,82,18]. Since synchrotron photons are inverse Compton scattered by their parent relativistic electrons, the Crab Nebula is considered to be a synchrotron-self-Compton source.

### *The Structure of the Nebula*

ROSAT and HST observations of synchrotron emission from the Crab Nebula led Hester et al. [43] to make the following fundamental observation about the structure of this nebula: almost all observations of the system at all scale sizes show a well-defined axis of cylindrical symmetry running from the south-east (SE) to the northwest (NW) through the center of the nebula, at an angle tilted by  $20^\circ - 30^\circ$  with respect to the plane of the sky. This axis corresponds to the direction of elongation of the nebula as a whole, the axis of the X-ray and optical jets, the X-ray torus (first identified by [3]) and the alignment of the optical “wisps.”

Hester et al. [43] also summarized the main properties of the pulsar wind which is responsible for the unpulsed emission over several decades in energy. The symmetry axis is probably associated with the pulsar spin axis, and the DC component of the rotating magnetic field results in a helical polar wind centered on the spin axis. The elongated optical synchrotron nebula appears to be associated with this high latitude structure. Equipartition between particle and field energy is probably reached in the optical nebula, with  $B_{\text{optical}} = 3 \times 10^{-4}$  G [43]. This optical nebula is also expected to be the source of IC TeV  $\gamma$ -rays [39,18]. In fact, TeV observations of the Crab Nebula did confirm a field strength of  $\sim 3 \times 10^{-4}$  G for the optical/TeV nebula [18]. Closer to the pulsar, [43] identified relatively small optical knots in the polar axis with equipartition field strengths as high as 2 mG, and [19] discussed the possibility that the variable structures near the pulsar may be associated with the variable  $\gamma$ -ray emission seen by EGRET (see also below).

The equatorial zone (identified as the X-ray torus by [3]) extends  $\sim \pm 10^\circ$  from the spin equator of the system, with a relatively low field (azimuthally wound up) strength distribution of  $B_{\text{torus}} \sim 7 \times 10^{-5}(r/8'')^{0.5}$  G for  $r > 8''$ , as derived by [11] from EINSTEIN HRI images. The X-ray emission up to at least 50 keV is associated with this torus [66], but above this energy we

have no imaging capabilities to identify the site of gamma-ray emission, and we have to rely on spectral and temporal characteristics to infer constraints on the properties of the gamma-ray emission site (see [19] for a more detailed discussion of the gamma-ray properties).

### *The high energy synchrotron tail*

CGRO probed the energy range above 50 keV where no imaging is possible, and a comparison between BATSE, OSSE, COMPTEL and EGRET observations of the Crab total emission was made by [62]. Whereas BATSE overestimated the the low energy gamma-ray flux, OSSE and COMPTEL produced consistent results below 1 MeV. The spectral steepening above  $\sim 100$  to 200 keV reported by [49] and [7] is confirmed by OSSE observations. This indicates that the toroidal component terminates gradually above  $\sim 200$  keV.

Conflicting results are however produced above  $\sim 1$  MeV: whereas COMPTEL observed a consistent spectral hardening above 1 MeV, OSSE observed this hardening only during Observation 221 [62]. The flux in the 1–30 MeV range also appears to be variable with time [61], and if this hardening is real, it would be indicative of the presence of another  $\gamma$ -ray emitting site. The rapid variability associated with this component was interpreted by [19] as an emission site near the pulsar where  $B \sim 0.1\mu\text{G}$ . Hester et al. [43] identified the optical knots near the pulsar as shock-like sites with  $B$  of the same order as required by De Jager et al. [19].

A comprehensive analysis of EGRET observations of the Crab Nebula was reported by [19] and it was shown that the hard COMPTEL component should cut off above  $\sim 25$  MeV to meet the steep EGRET spectrum between 70 MeV and 150 MeV. De Jager et al. [19] interpreted the steep spectrum between 30 MeV and 150 MeV as the exponential tail of the synchrotron cutoff in the Crab Nebula. The e-folding energy at 25 MeV is consistent with the interpretation that electron acceleration in a relativistic shock occurs at a rate equal to the gyrofrequency. This acceleration is constrained by synchrotron losses, and it was shown that the synchrotron characteristic energy associated with the highest electron energy is independent of the magnetic field strength, and depends only on fundamental constants and a factor  $\epsilon \sim 1$  which depends on the Doppler factor and the average electron pitch angle. Thus,

$$h\nu_{\text{max}} = \epsilon \left( \frac{3}{4\pi} \right)^2 \frac{hc}{r_e} = \epsilon \frac{9}{8\pi} \frac{m_e c^2}{\alpha_f} \approx 25\epsilon \text{ MeV}, \quad (1)$$

where  $r_e$  is the classical electron radius and  $\alpha_f$  is the fine structure constant.

Furthermore, this EGRET component was also found to be variable on a timescale similar to the COMPTEL variability timescale. Thus, whereas the stable emission below 1 MeV is known to be associated with the torus, the variable hard component associated with the synchrotron cutoff leads to the

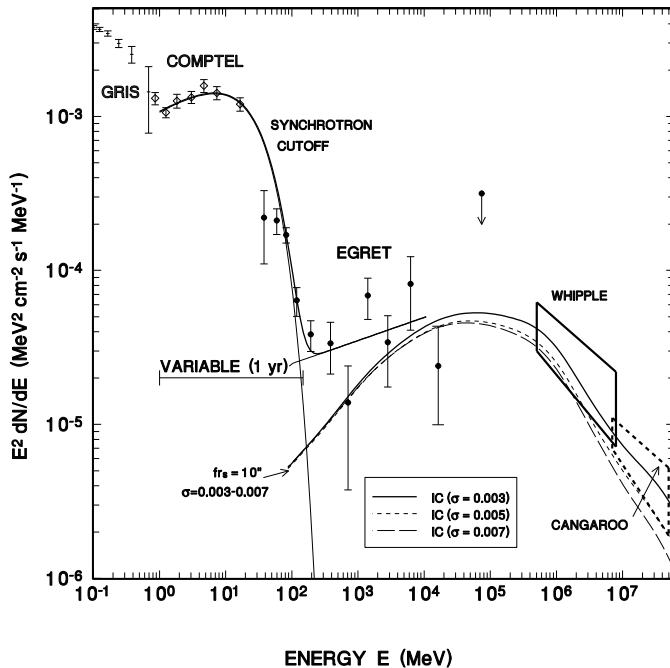


**FIGURE 1.** The Crab nebular unpulsed  $\gamma$ -ray spectrum ( $E^2 dN/dE$ ) in the energy range 0.1 MeV to 20 TeV. The references are: GRIS [7], COMPTEL [61], & EGRET [19]. References to TeV points are given by [19]. The Whipple error box (including systematic and statistical errors) is from [16], and the CANGAROO error box is from [70]. A two-component fit (1-150 MeV) resulted in a power law with an exponential cutoff at 25 MeV, and an inflection point at 150 MeV. The inverse Compton model of [18] was used to generate spectra for  $r_s = 10''$  and three values of  $\sigma$  (as labelled), as shown for energies between 100 MeV and 20 TeV. The model uncertainty is a factor 2 at any energy.

conclusion of an association with a high-B region close to the pulsar, which is removed from the torus. The polar region where high-B optical knots and variable “anvil” is found, is therefore a candidate region for this variable hard component. However, future  $\gamma$ -ray observations above 1 MeV with improved calibration is required to confirm these findings.

### *The Inverse Compton component*

Above  $\sim 150$  MeV, [19] found a steady hard component, which steepens gradually to meet the very high energy spectral points above 100 GeV (see Fig. 1). This steady hard component was predicted to be the inverse Compton component. The *relic* radio emitting electrons also scatter the optical background photons into the  $\sim 100$  MeV to GeV energy range, whereas the younger optical and X-ray emitting electrons are expected to be responsible for the TeV  $\gamma$ -rays. The lifetimes of the radio to X-ray emitting electrons

are much longer than the timescale of gamma-ray observations, which implies that we should not expect to see a variable inverse Compton  $\gamma$ -ray component. The observed  $\gamma$ -ray flux above 150 MeV was found to be larger than predicted by the synchrotron-self-Compton model [19]. The EGRET  $\gamma$ -rays above 150 MeV may be associated with inverse Compton  $\gamma$ -ray emission if the field strength in the larger radio nebula is  $\sim 1.3 \times 10^{-4}$  G, which is smaller than the field strength in the smaller optical/TeV nebula. This would suggest a departure from the nebular field distribution derived by [51].

## The Vela Supernova remnant

The Vela Supernova remnant appears to be associated with the Vela pulsar PSR B0833-45, which has a spindown age of about 11,000 years. A large-scale *ROSAT* image of thermal soft X-rays ( $kT = 0.12$  keV) from the Vela SNR shows that the diameter of the remnant is  $7.3^\circ$ , with the pulsar at its center. In hard X-rays we do not see this thermal shell. Rather, the synchrotron nebula is resolved into an elongated (NE-SW) hard X-ray (2.5 - 10 keV) structure as shown by [83], and a compact nebula surrounding the pulsar. The energy-dependent geometry of this remnant was illustrated in Fig. 1 of [21].

### *The OSSE detection of Vela*

Fig. 2 shows the non-thermal X-ray to low energy gamma-ray spectrum of the 1 arcmin compact synchrotron nebula around the Vela pulsar as seen by ROSAT, EINSTEIN, Birmingham and possibly OSSE as reported by [21] and [74]. Even though the OSSE instrument does not have imaging capabilities for a clear association, the spectra of other X-ray sources in the field-of-view cut off below the OSSE range, and only the Vela SNR remains as candidate. Furthermore, since the OSSE spectrum connects smoothly with the lower energy X-ray (imaging) spectra, the association is quite likely. The authors have also shown that the energetics of electrons (given the field strength scaled from the pulsar) is sufficient to produce  $\gamma$ -rays into the low energy part of the EGRET range (Fig. 2). The unbroken spectrum and the EGRET upper limit constrain the maximum electron energy to values smaller than those expected from the  $3 \times 10^{15}$  volt polar cap potential drop. More sensitive observations above 400 keV are needed to measure the cutoff energy, which should lead to a measurement of the maximum electron energy in the nebula.

### *An inverse Compton component from Vela X?*

The relatively hard spectrum associated with the bright Vela X radio nebula (about  $1^\circ$  south of the pulsar) represents synchrotron emission from relic

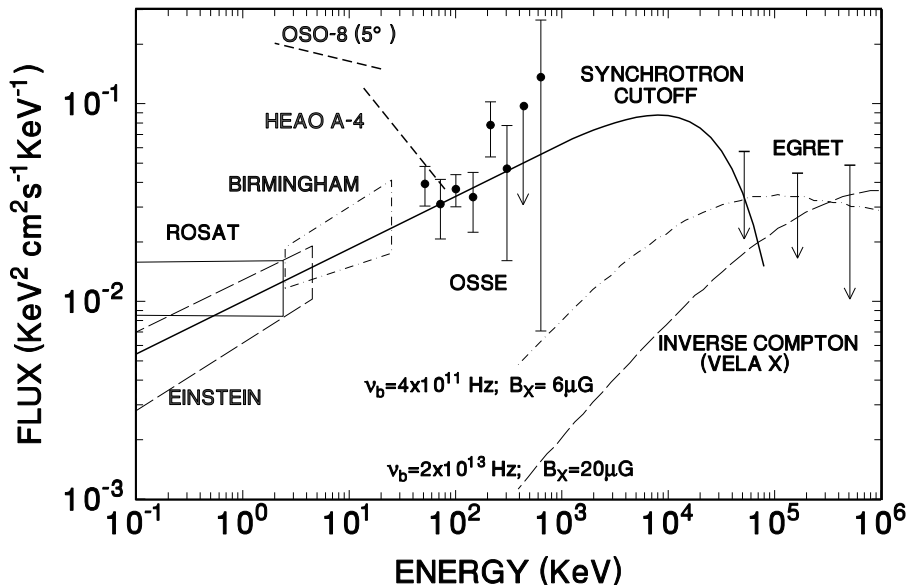


**FIGURE 2.** The EINSTEIN, ROSAT, & Birmingham X-ray spectra of the 1' Vela compact nebula (see [21] for references). See also ref. [21] for the corresponding OSSE spectrum of the Vela 1' radius compact nebula. The 30-100 MeV EGRET upper limit constrains the extent of this spectrum to an e-folding cutoff energy  $< 40$  MeV [20]. EGRET upper limits above 100 MeV constrain the inverse Compton contribution from Vela X, with the break frequency  $\nu_b$  and field strength  $B_X$  as free parameters. Two such Vela X spectra constrained by EGRET are shown by the dot-dash and long dashed lines (see ref. [20] for details).

electrons in the nebula, while the inverse Compton emission resulting from the scattering of the 2.7K cosmic microwave background produces MeV to GeV  $\gamma$ -rays. This component would be observable if the electron concentration in the Vela X remnant were sufficient. However, we only know the synchrotron brightness of Vela X, which represents a combination of the electron concentration and the magnetic field distribution. A search for emission in the EGRET data base revealed marginal evidence for excess emission from this direction. De Jager et al. [20] have shown that we should not expect to see MeV to GeV inverse Compton  $\gamma$ -rays from the Vela X SNR if the particles and fields are in equipartition with  $B \sim 30\mu\text{G}$ . This is consistent with the EGRET upper limits, which lie above the flux expected for equipartition.

Fig.2 shows some non-equilibrium inverse Compton spectra which are just below the EGRET upper limits, and it is clear that we must know the maximum electron energy (which is seen as a cutoff at a frequency  $\nu_b$  in the radio spectrum) before we can give a meaningful lower limit on  $B$ . Unfortunately the detection of  $\nu_b$  in the radio to far-infrared region is hampered by the

presence of dust emission in the far IR. Again, a next generation gamma-ray observatory may lead to a detection of Vela X, which should allow a more detailed study of the parameters involved.

### *Relic electrons at the birthplace of the Vela pulsar?*

The CANGAROO telescope has reported unpulsed emission above 2.5 TeV from the Vela pulsar. The peak of this emission is located 8' southeast of the pulsar, which is the projected birthplace of the pulsar, given the 11,000 year spindown age of the pulsar, and the observed proper motion vector [85]. A hint of radio emission at this birthplace is also seen (Frail, D.A. 1996, private communication). Using archival ASCA data, Harding et al. [41] have shown that the X-ray and TeV  $\gamma$ -ray observations indicate the presence of relic electrons left in the trail of the moving pulsar if the magnetic field strength at this site is between 1.3 and 3  $\mu$ G. Such a low field would have allowed electrons to have survived since the birth of the pulsar. While the X-ray emission is the result of synchrotron emission from relic TeV electrons in a weak field, the TeV  $\gamma$ -ray emission results from the inverse Compton scattering of the same electrons on the cosmic microwave background.

### **The Unpulsed TeV Source: PSR B1706-44.**

Frail, Goss & Whiteoak [35] identified a 4' halo ( $\sim 60$  mJy flux density at 1.5 GHz) of extended plerionic radio emission around the pulsar PSR1706-44. The 20' trailing emission, which, if attributed to proper motion effects, implies that the pulsar and SNR G343.1-2.3 are not associated. Becker, Brazier, & Trümper [8] identified unpulsed power law ( $\alpha_x = 1.4 \pm 0.6$  energy index) X-ray emission from this pulsar, with a spatial extent which is consistent with the  $\sim 0.5'$  spatial resolution of the ROSAT PSPC. No soft X-ray emission has been detected from the 4' radio halo, and Becker, Brazier, & Trümper [8] made the point that the unresolved X-ray source associated with this pulsar is a compact nebula, similar to the compact nebula of the Vela pulsar.

This pulsar was also seen to be emitting unpulsed TeV  $\gamma$ -rays [54], similar to the Vela TeV detection, which strengthens the conclusion of the similarity between the Vela and PSR1706-44 compact nebulae. However, no unpulsed  $\gamma$ -ray emission in the CGRO range was seen from the direction of PSR1706-44, and the pulsed flux from the pulsar is consistent with the total flux in the EGRET range [80]. The non-detection of  $\gamma$ -rays in the CGRO range is not surprising: any OSSE type emission is expected to be  $\sim 10$  times weaker than the corresponding flux seen from Vela, given the larger distance to PSR1706-44 and similar source parameters. The absence of a radio synchrotron nebula due to relic electrons would also rule out the possibility of an inverse Compton component in the 100 MeV to 1 GeV range.



## W44: A COMPOSITE (SHELL + PLERIONIC) SNR

The previous discussion was concerned with the detection of gamma-rays from pulsar-injected electrons (plerions). Some remnants are composite, exhibiting both pulsar/plerionic and shell structures, and we may expect an interesting interaction of electrons injected by the pulsar into the shell, where further electron acceleration may take place, resulting in a bright radio shell. If this remnant is also interacting with a molecular cloud, we may expect relativistic bremsstrahlung to produce gamma-rays in addition to inverse Compton scattering. Furthermore, a  $\gamma$ -ray component from cosmic ray proton acceleration in the shell may also be expected. In fact, the EGRET instrument on the Compton Gamma Ray Observatory detected high energy  $\gamma$ -rays from the vicinity of radio-bright shell-type supernova remnants  $\gamma$  Cygni, IC443, W44 and W28 [34]. These remnants are all associated with molecular clouds, which provide the natural target material for the production of  $\gamma$ -rays via either relativistic bremsstrahlung, or the spallation products of proton-gas interactions (discussed below).

### Morphological properties of W44

Fig. 4b (see next section) gives us an indication of the morphology of W44: The EGRET  $\gamma$ -ray source 2EG J1857+0118 [80,34] is located on the eastern side of this remnant, and from Fig. 1 of [22] it is clear that this remnant is also interacting with a molecular cloud on the eastern side, as inferred from  $^{13}\text{CO}$  and other molecular line observations [84,24]. The presence of  $^{13}\text{CO}$  is indicative of gas densities in excess of  $10^3 \text{ cm}^{-3}$  in localized interstellar “baseballs,” whereas the inter-clump densities are of the order of  $\sim 1 \text{ cm}^{-3}$  or less [69]. De Jager & Mastichiadis [22] found an average hydrogen density of  $\sim 50 \text{ cm}^{-3}$  in the shell of the remnant, which is large enough for the production of  $\gamma$ -rays via various processes.

Whereas the radio is shell-like, the X-ray emission [69] is centrally-peaked, with the radio pulsar PSR B1853+01 offset from the center of the remnant. The association of the pulsar with the remnant is strengthened by the detection of a weak cometary tail (the pulsar wind nebula) pointing towards the center of the remnant [36]. The transverse speed of the pulsar is comparable to the expansion speed of the radio shell [36]. Harrus, Hughes, & Helfand [42] also discovered a smaller X-ray PWN, but the luminosity of the PWN is however negligible compared to the total X-ray luminosity of W44. Arendt [2] identified infrared emission from W44, showing a good spatial correlation with W44. This emission is probably a result of swept-up dust during the SNR expansion, and the infrared energy density is larger than the other galactic radiation fields [22]. This radiation field was included in the inverse Compton calculations of de Jager & Mastichiadis [22].

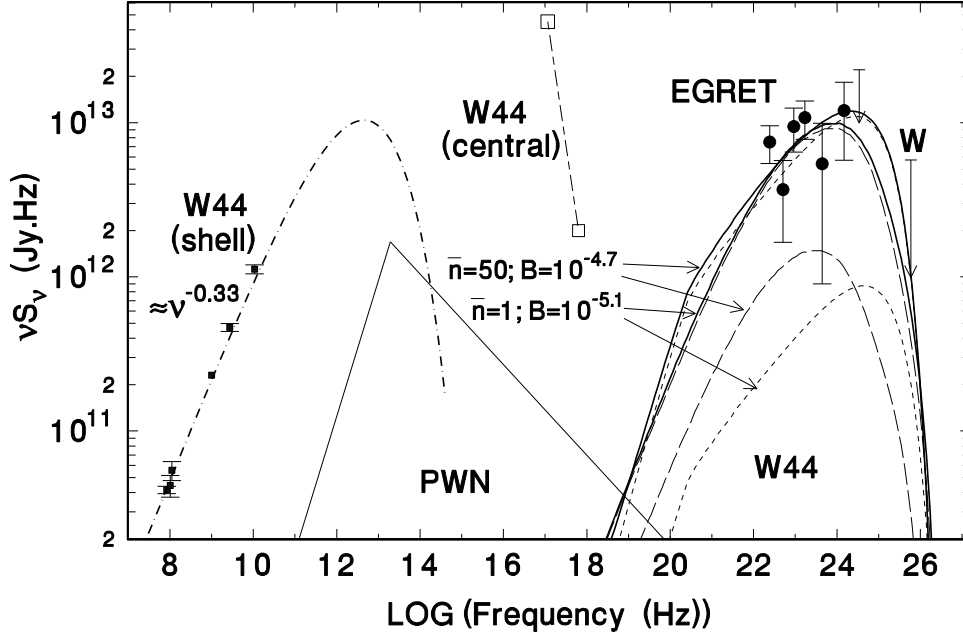


**FIGURE 3.** The observed multiwavelength spectrum of W44. See ref. [22] for references to data/model fits at all wavelengths. The dot-dash line indicates a model fit to the radio data, which includes a cutoff at  $\nu_b = 3 \times 10^{12}$  Hz; open boxes — thermal X-ray energy fluxes of W44 (the thermal turnover at  $\nu < kT/h$  is not included); solid circles with error bars — EGRET energy fluxes; upper limit “W” — Whipple upper limit at  $\nu = 9 \times 10^{25}$  Hz. *Observed synchrotron spectrum of the pulsar wind nebula:* solid triangle with base between  $10^{11}$  Hz and  $10^{20}$  Hz, with intersection at  $\nu_p = 2 \times 10^{13}$  Hz. *Fits to  $\gamma$ -ray data* (for two choices of  $\bar{n}$  and  $B$  as indicated): short dashed lines — relativistic bremsstrahlung; long dashed lines — inverse Compton; thick solid lines — bremsstrahlung + inverse Compton.

## Spectral properties of W44

Fig. 3 shows the spectral properties of W44 as summarized by [22]. The emission from the shell dominates the pulsar emission (indicated by “PWN” in Fig. 3). Whereas the weak radio/X-ray plerionic component is non-thermal, only the radio component of the bright shell is non-thermal. The absence of non-thermal X-ray emission associated with the shell indicates that the radio spectrum must terminate at frequencies  $\ll 10^{16}$  Hz. The dot-dash line in Fig. 3 is a model fit through the radio spectrum, and the turnover at  $3 \times 10^{12}$  Hz (constrained by TeV  $\gamma$ -ray observations) assumes an exponential cutoff in the electron spectrum as discussed by [22].

## The bremsstrahlung/inverse Compton origin of 2EG J1857+0118

De Jager & Mastichiadis [22] have shown that the same electrons that are responsible for the radio emission can also explain the observed EGRET  $\gamma$ -ray spectrum between 70 MeV and 10 GeV. *The required cutoff in the high frequency radio spectrum accounts for the non-detection of W44 in non-thermal X-rays [69] and TeV  $\gamma$ -rays [58].* This emission is expected to be concentrated towards the eastern shell where the molecular densities are highest. The dust emission will also contribute to a weaker inverse Compton component [22].

The maximum electron energy in the shell, as derived from multiwavelength observations, is (in terms of the characteristic synchrotron frequency  $\nu_{12}$  corresponding to the cutoff frequency  $\nu_b$ )

$$E_{\max} = 0.14 (B_{-5})^{-1/2} \nu_{12}^{1/2} \text{ ergs.} \quad (2)$$

This maximum energy is orders of magnitude below the maximum obtained for SN1006 - another shell remnant which shows evidence for electron acceleration [59]. The uncertainty in the exact hydrogen density makes it difficult to infer the magnetic field strength from coupled synchrotron and bremsstrahlung equations, but values around  $10\mu\text{G}$  are expected given the approximate hydrogen densities. De Jager & Mastichiadis [22] also found that inverse Compton scattering dominates relativistic bremsstrahlung for molecular densities around 1 particle  $\text{cm}^{-3}$ , whereas bremsstrahlung dominates for  $\bar{n} \sim 50 \text{ cm}^{-3}$ , the density expected for this remnant.

### The implications of $\gamma$ -rays from W44

By integrating the electron energy spectrum up to the maximum electron energy, [22] obtained a total electron energy content of  $E_{\text{el}} = 5.8 \times 10^{49} B_{-5}^{-1.33}$  ergs, which is about 6 times larger than the value found for SN1006 by [59]. The conversion efficiency ( $\eta_{\text{el}} = E_{\text{el}}/E_{\text{SN}}$ ) of SN explosion energy  $E_{\text{SN}} = 6.7 \times 10^{50}$  ergs to electrons is then

$$\eta_{\text{el}} = 0.087 \left[ \frac{6.7 \times 10^{50} \text{ ergs}}{E_{\text{SN}}} \right] B_{-5}^{-1.33}, \quad (3)$$

which is relatively high for primary electron acceleration in SNR shocks [32,60]. De Jager & Mastichiadis [22] addressed this problem by investigating the total output from the pulsar PSRB1853+01 since the birth of this  $\sim 20,000$  year old SNR. They found that the shell electrons which we are now seeing in radio and  $\gamma$ -ray emission, may have been the result of relic electrons which have been injected into the SNR since birth, provided that the initial spindown power of the pulsar exceeded the present spindown power of the Crab pulsar.

Further support for this interpretation comes from the fact that the radio (and hence electron) spectrum of the shell of W44 is hard and Crab-like, rather than reminiscent of the softer shell-type spectra. Thus, the radio/ $\gamma$ -ray spectrum of the shell of W44 may be the result of relic Crab-like electrons injected into the shell of W44 during the past 20,000 years.

Proton – gas interactions may result in the production of pions from which  $\gamma$ -rays are expected (see below). This process is believed to account for the  $\gamma$ -ray emission from shell remnants interacting with molecular clouds as observed by EGRET. De Jager & Mastichiadis [22] have however shown that the average gas density in W44 is not sufficient to account for a dominant proton contribution to the EGRET  $\gamma$ -rays, and the contribution from this hadronic component is probably not more than 20%. Extrapolation of this relatively weak component to the TeV range may also account for the unobservability of W44 at TeV energies, regardless of whether or not wave damping due to neutrals [26] truncates the proton spectrum below the TeV range.

## SHELL-TYPE SUPERNOVA REMNANTS

It has been widely-perceived that supernova remnants (SNRs) are a principal, if not the predominant, source of galactic cosmic rays (e.g. see [57]) up to energies of around  $\sim 10^{15}$  eV, where the so-called *knee* in the spectrum marks its deviation from almost pure power-law behaviour. Such cosmic rays are presumed to be produced by diffusive shock (Fermi) acceleration in the environs of supernova shocks. Remnants are a convenient origin for cosmic rays below the knee because their ages (between 100 and  $10^5$  years) and sizes permit the diffusive process to accelerate up to such high energies, they have the necessary power to amply satisfy cosmic ray energetics requirements, and current estimates of supernova rates in our galaxy can adequately supply the observed cosmic ray density (e.g. see [10]).

The evidence for cosmic ray acceleration in remnants is, of course, circumstantial. Nevertheless, the ubiquity of polarized, non-thermal radio emission in remnants (e.g. see references in the SNR compendium of Green [40]) argues convincingly for efficient acceleration of electrons if the synchrotron mechanism is assumed responsible for the emission. X-rays also abound in remnants, and are usually attributed to thermal emission from shock-heated electrons (because of the appearance of spectral lines, e.g. see [12] for Cas A). The striking spatial coincidence of radio and X-ray images of shell-type remnants (e.g. Tycho [10] and SN1006; see [52] for a radio/X-ray correlation analysis for Cas A) suggests that the same mechanism is responsible for emission in both wavebands. This contention has recently received a major boost with the discovery of non-thermal X-ray emission in SN1006 [56], which implies [68] the presence of non-thermal electrons at super TeV energies. In addition, very recent ASCA spectra (Keohane et al. [53]) for the remnant IC 443 and

RXTE observations of Cas A (Allen et al. [1]) exhibit non-thermal X-ray contributions, adding to the collection of super-TeV electron-accelerators. A nice review of radio and X-ray properties of SNRs is given in [33].

A product of cosmic ray acceleration in SNRs is that such energetic particles can generate gamma-rays via interactions with the ambient interstellar medium (ISM), just as in models of the diffuse gamma-ray background [45,46]. Despite theorists' early expectations [44,17] that remnants will be gamma-ray bright, no definitive detection of such emission from a supernova remnant has been reported. Prior to the launch of CGRO, associations of remnants with gamma-ray sources has been limited to two unidentified COS-B sources [67] (for  $\gamma$ -Cygni and W28), however CGRO has played an important role in advancing this field. Our emphasis in the discussions below will be on shell-type remnants such as  $\gamma$ -Cygni, IC 443 and W28.

## Gamma-Ray Observations in the CGRO Era

The potential importance of the Compton Observatory's contribution to the study of supernova remnants was identified on a theoretical level by Drury, Aharonian and Völk [27], and in an observational context by Sturmer and Dermer [75] in relation to unidentified (UID) EGRET sources. While [75] indicated that the latitudinal distribution of the UID sources may suggest a supernova origin (discussed more extensively in [64]), it was also pointed out that the chance probability of coincidental association for a handful of unidentified EGRET sources with known radio SNR counterparts was small. The best candidates for such associations are presented in the work of Esposito et al. [34], who focused on unidentified EGRET sources (with approximately  $E^{-2}$  spectra at above 100 MeV) in or near the galactic plane and proximate to relatively young radio/optical/X-ray-emitting remnants. Such associations, which are at first glance very enticing, suffer from the large uncertainty [34] in exact directional location of the (assumed point) sources for the EGRET detections, of the order of 0.5–1 degrees, i.e. the size of typical nearby remnants (see the images depicted in Figure 4). Hence a definitive connection between *any* of these gamma-ray sources and the young SNRs is not yet possible.

The situation is complicated by the presence of a pulsar (PSR B1853+01) in the field [34,22] of the 95% confidence contour of the EGRET source 2EG J1857+0118, whose association with the remnant, W44, is discussed above. Such a pulsar, or its wind nebula, could easily generate the observed gamma-ray emission, although no evidence of pulsation exists in the EGRET data [79]. There is also the recent suggestion [14] of a pulsar counterpart to the CTA 1 remnant's EGRET source 2EG J0008+7307. In addition, the improvement of the localization of 2EG J2020+4026 by the consideration of only super-GeV photons leads to the conjecture [13] that this source is not associated with the shell of  $\gamma$  Cygni, but rather with a distinct ROSAT source that may also be a

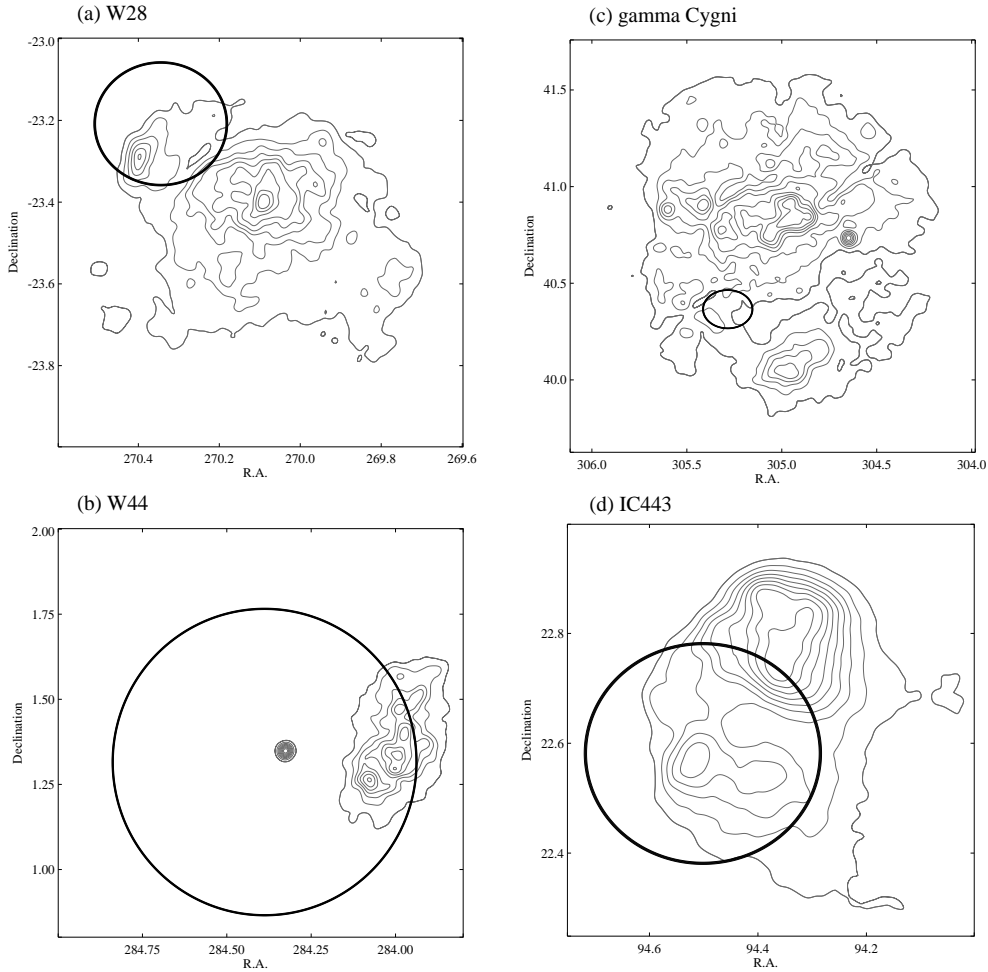


**FIGURE 4.** The X-ray/gamma-ray images of the supernova remnants W28, W44,  $\gamma$ -Cygni and IC443, as presented in Esposito et al. [34]. These consist of X-ray contours from the ROSAT telescope’s HRI, and the 95% (elliptical) confidence contours of emission above 100 MeV in the associated EGRET unidentified sources.

pulsar. The possibility that pulsars could be responsible for most unidentified EGRET sources near the galactic plane [50] (see also [64]) currently precludes any assertions stronger than just suggestions of a remnant/EGRET source connection. Notwithstanding, it is quite possible that such remnants could plausibly emit gamma-rays at levels below EGRET’s sensitivity.

The absence of TeV emission associated with the remnants surveyed by Esposito et al. [34], as reported by the Whipple collaboration [58,15], is as important for this field as the detections embodied in the EGRET unidentified sources. Upper limits obtained by Whipple to a number of remnants can severely constrain models, dramatically impacting the hypothesized contributions of hadronic processes, bremsstrahlung and inverse Compton scattering. Very recently, the CANGAROO experiment detected [78,55] the barrel-shaped

remnant SN1006 above 3 TeV, a source for which the existence of highly super-TeV electrons has already been established [56,68] from the X-rays. Future observations in the TeV band will provide powerful model diagnostics.

## Modelling of Gamma-Ray Production in SNRs

The modelling of  $\gamma$ -ray emission from supernova remnants was limited to a few very preliminary analyses (e.g. [44,17,9]) prior to the launch of CGRO. This field of research began in earnest with the seminal paper of Drury, Aharonian and Völk [27], who computed (as did ref. [65]) the photon spectra expected from the decay of neutral pions generated in collisions between shock-accelerated ions and cold ions in the ISM. Since then, there has been a small flurry of activity, with different groups using alternative approaches, extending the considerations to include bremsstrahlung and inverse Compton emission. Here we review the handful of SNR gamma-ray emission models developed over the last four years that invoke shock acceleration.

Drury et al. [27], determined the photon spectra and fluxes expected from the decay  $\pi^0 \rightarrow \gamma\gamma$  of neutral pions generated in hadronic collisions ( $pp \rightarrow p\pi^0 X$  etc.) between power-law shock-accelerated ions and cold ions in the ISM; they neglected the other (electromagnetic) processes mentioned just above. Due to the isotropy of decay in the pion rest frame, the decay kinematics yield [72] a photon spectrum that is symmetric about  $m_\pi/2 \approx 67$  MeV, an unmistakable signature of the production of pions in astrophysical systems (see [45,46] for its role in determining the gamma-ray background spectrum). Supernova remnant models of pion production and decay normally use some variant of a hybrid approach (e.g. see Dermer [23]), where low energy pion creation (for shock-accelerated proton momenta  $p_p$  below around 3 GeV/c) is mediated by an isobaric state  $\Delta(1232)$  (Stecker [72]), or a collection of different states, and the complexities of pion creation at high energies (for  $p_p \gtrsim 10$  GeV/c) is described by some adaptation [73,77] of Feynman scaling. Drury et al. used the *two-fluid* approach [28,25,4] to explore shock acceleration hydrodynamics, treating the cosmic rays and thermal ions as separate entities (electrons go along for the ride). This technique, which is extremely useful for time-dependent problems such as SNR expansions, obtains solutions that conserve particle number, momentum and energy fluxes, thereby describing some of the non-linear effects [47,4] of diffusive shock acceleration. Drury et al. determined that the luminosity peaked in the Sedov phase, in accord with maximal shock dissipation arising when the supernova ejecta is being compressed and significantly decelerated by the ISM.

In order to match the EGRET flux, Drury et al.'s pion decay model requires a *high target density* ( $> 100 \text{ cm}^{-3}$ ). Gamma-ray bright remnants might therefore be expected to border or impinge upon dense regions of the ISM, perhaps giant molecular clouds, in accord with the earlier suggestions of [9].

Drury et al. [27] predicted that such remnants should become limb-brightened with age, an effect that arises because, as the shock weakens with time, the dominant  $\gamma$ -ray flux is always “tied” somewhat to a region near the shock. While such a limb-brightening is seen in radio and X-ray images of remnants (e.g. Tycho and SN1006), higher angular resolution observations are needed in gamma-ray telescopes before its existence, or otherwise, can be probed at high energies. Such a definitive connection of the  $\gamma$ -ray emitting regions to a remnant’s shell (which may be ruled out for  $\gamma$  Cygni according to [13]) would argue strongly for a shock-acceleration origin of the energetic particles responsible for emission in the gamma-ray and other wavebands. Note that Drury et al. did not incorporate physical (spatial and temporal) limits imposed [57,59,68,4,6] on the shock acceleration mechanism by the supernova shell, so that they permitted particles to be accelerated to at least 100 TeV. This omission promoted observational investigations by the Whipple collaboration that produced upper limits in the TeV energy range [58,15] that contradicted the Drury et al. predictions. While this conflict has been proposed as a failure for shock acceleration models of SNRs, realistic choices [22,76,6] of the maximum energy  $E_{\max}$  of particle acceleration actually yield model spectra that are quite compatible with Whipple’s observational constraints to  $\gamma$  Cygni and IC 443.

A number of substantial model developments has ensued since Drury et al.’s enunciative work. Among these was the work of Gaisser, Protheroe and Stanev [37]. They computed emission fluxes and luminosities for the decay of  $\pi^0$ s produced in hadronic collisions, bremsstrahlung and inverse Compton scattering, however they omitted consideration of non-linear shock dynamics in any form, did not treat time-dependence, and assumed test-particle power-law distributions of protons and electrons. In their model, the inverse Compton scattering used both the microwave background and an infrared/optical background field local to the SNRs as seed soft photons. Their bremsstrahlung component was due to cosmic ray electrons colliding with ISM protons. Their model has difficulty with the TeV upper limits obtained by Whipple, unless sufficiently steep particle distributions are assumed. Gaisser et al. imposed a high matter density ( $> 300 \text{ cm}^{-3}$ ) to enhance the bremsstrahlung and  $\pi^0$  decay to inverse Compton flux ratio, thereby generating steeper spectra for the sources associated with  $\gamma$  Cygni and IC443. Note that for all models discussed here, the  $\pi^\pm \rightarrow e^\pm$  secondaries are always unimportant for the SNR problem since the ion cooling time in pion production is much longer than typical remnant ages.

Recently Sturmer et al. [76] have developed a time-dependent model, where they solve for electron and proton distributions subject to cooling by inverse Compton scattering, bremsstrahlung,  $\pi^0$  decay and synchrotron radiation. Like Gaisser et al., the work of Sturmer et al. assumes canonical power-laws but does not include any treatment of non-linear shock acceleration effects. One feature of their model is the dominance of inverse Compton emission, which



intrinsically has a flatter spectrum than either bremsstrahlung or pion decay radiation. This arises because they generally opt to have the same energy density in non-thermal electrons and protons, so that the shock-accelerated electrons are more populous than their proton counterparts. Sturmer et al.'s work introduced cutoffs in the distributions of the accelerated particles (first done by [59]), which are defined by the limits on the achievable energies  $E_{\max}$  in Fermi acceleration. Hence, given suitable model parameters, Sturmer et al. can accommodate the constraints imposed by Whipple's upper limits [58] to  $\gamma$  Cygni and IC 443.

The most recent development among gamma-ray production models has been the work of Baring et al. [5,6] on the application of non-linear shock acceleration theory to the SNR problem, an appropriate step given that remnant shocks are strong enough that the generated cosmic rays are endowed with a significant fraction of the total particle pressure. This work utilizes the steady-state Monte Carlo simulational approach (described in the reviews of [47,4]), a kinematic technique that can self-consistently model the feedback of the accelerated particles on the spatial profile of the flow velocity, which in turn determines the shape of the particle distribution. In establishing this feedback, the accelerated population pushes on the upstream plasma and decelerates it before the discontinuity is reached, so that an upstream *precursor* forms, in which the flow speed is monotonically decreasing. At the same time, the cosmic rays press on the downstream gas, slowing it down too. The overall effect is one where the total compression ratio  $r$ , from far upstream to far downstream of the discontinuity, actually *exceeds that* (i.e. 4) *of the test-particle scenario*, the case where the canonical power-laws used in [27,37,76] are generated. This situation results from the need of the flow to increase  $r$  to adjust for energy and momentum escape [29,31]. If the particle diffusive scale (i.e. mean free path  $\lambda$ ) is an increasing function of momentum, as is expected to be the case [4] based on inferences of particle diffusion from the Earth's bow shock and also in hybrid plasma shock simulations [38], then higher energy particles will sample a stronger shock, yielding upward curvature in the non-thermal cosmic ray distribution. This curvature is important for gamma-ray emission models, since it introduces enhancements [5] in the TeV range by factors of 2–3 relative to the EGRET range; such increases can be the difference between detection and non-detection by air Čerenkov experiments like Whipple, CAT, CANGAROO and HEGRA. The curvature and the modification of the flow hydrodynamics depend on each other intimately in a highly non-linear fashion. Typical distributions of particles that are accelerated in *cosmic ray modified* shocks are presented in numerous papers [29,31,47,30,6].

The self-consistent Monte Carlo approach to shock acceleration in [6] includes neutral pion decay emission, bremsstrahlung and inverse Compton emission components. The cessation of acceleration above  $E_{\max} \sim 1$  TeV - 10 TeV range caused by the spatial and temporal limitations of the expanding SNR shell yields gamma-ray spectral cutoffs that are consistent with the

Whipple TeV upper limits [58,15]. The Monte Carlo approach generates particle diffusion scales that are always much less than the remnant's shock radius (as in [27]) so that the effects of shock curvature can be neglected. This may also render the lack of time-dependence in the technique a less relevant limitation. A prominent feature of the model of [6] is the low value of the electron to proton ratio above 1 GeV, due to a sensible description of the injection of thermal electrons into the acceleration process. This description, which models the way particles diffuse in turbulent plasma environments, guarantees [4] that the electron distribution is steep enough at low energies so as to render the  $e/p$  ratio much less than unity above 1 GeV. This determination is entirely consistent with the observation that electrons supply around 2% of the cosmic ray population by number [63], and also blends with limits on the local  $e/p$  abundance ratio imposed when modelling the galactic gamma-ray background [45]. This contrasts the situation of [76]. Note that while bremsstrahlung is more efficient than pion decay emission for given cosmic ray electron and proton energies, the emergent bremsstrahlung component can be inhibited if the  $e/p$  ratio is low. Future measurements of the unidentified sources by more sensitive experiments in the 1–100 MeV range should constrain the  $e/p$  ratio.

While the focus here has been on gamma-rays from shell-type remnants, much can be learned from studying other wavebands also. This has been the approach of Mastichiadis and De Jager [59], who have studied the remnant SN1006. For SN1006, which has not been seen in gamma-rays, they used [59] the recent observations [56] of non-thermal X-rays by ASCA to constrain the energy of electrons and the magnetic field, interpreting the X-ray flux as being of synchrotron origin. This contention (see also Reynolds [68]) assumes that the steep X-ray spectrum is part of a rollover in the electron distribution at energies around 100 TeV. Using microwave and infrared backgrounds appropriate to SN1006, [59] predicted the resulting inverse Compton component in  $\gamma$ -rays, and determined that it would always satisfy the EGRET upper bounds. However, they concluded that TeV upper limits from experiments like Whipple could potentially constrain the ratio  $\eta = \lambda/r_g$  of the electron mean free path  $\lambda$  to its gyroradius  $r_g$  to values signifying departure from Bohm diffusion (i.e.  $\eta \gg 1$ ), otherwise the TeV flux would exceed that of the Crab nebula. Such a conclusion appears to be borne out by the very recent announcement by Tanimori et al. [78,55] of the detection of SN1006 above 3 TeV by the CANGAROO experiment, with the flux at these energies probably being due to an inverse Compton component. Pinning the X-ray synchrotron spectrum determines  $E_{\max}^2 B$  and also a combination of  $B$  and the electron density, where  $E_{\max}$  is the maximum accelerated electron energy. Through  $E_{\max}$ ,  $\eta$  couples to  $B$  so that the gamma-ray inverse Compton flux anticorrelates with both  $B$  and  $\eta = \lambda/r_g$ . This interplay between the wavebands (see also [76]) will play an important role in future model developments for shell-type remnants.

## CONCLUSION AND A LOOK AHEAD

The Compton Gamma-Ray Observatory has propelled the study of supernova remnants, plerionic and non-plerionic, into the foreground of gamma-ray astrophysics. The various aspects of the plerions, the shell-type remnants, and the W44 composite discussed in this review serve to underline the diversity of the handful of definitive or candidate  $\gamma$ -ray remnants observed by CGRO. Such a diversity is also reflected in their morphological properties, their optical/IR spectra, environmental densities, etc. It follows that no two sources seem the same so that they must be considered on a case-by-case basis. While the plerions can easily derive their luminosity from the parent pulsar, perhaps the proximity of the non-plerionic sources to dense molecular clouds of various sorts provides a strong clue to the reason for their  $\gamma$ -ray emission. It is clear that if some of the EGRET detections turn out to be of gamma-rays generated in the environs of remnant shells, then gamma-ray emitters must be a minority of remnants, perhaps mostly young, given that they cannot produce ions above around a few TeV in profusion. Remnants that provide cosmic rays up to the knee must consequently be a gamma-ray quiet majority. Alternatively, if fluxes of shell origin are well below EGRET's flux sensitivity, then the notion that shell-type remnants are simultaneously gamma-ray bright and prolific producers of cosmic rays becomes tenable. It has therefore become evident that the Whipple upper limits have not destroyed the hypothesis that shocks in shell-type remnants energize the particles responsible for the gamma-ray emission, but rather have provided a powerful tool for constraining our understanding. Much remains to be explored in this field, in particular the relationship between the clouds and the shock parameters, the degree of ionization of the environment, the precise location of the gamma-ray emission, differentiation between plerion-driven and shock-powered gamma-ray sources, and the maximum energies and relative abundances of the produced cosmic rays. The next generation of both space-based and ground-based gamma-ray telescopes, with better angular resolution and cumulatively-broad spectral range will have a significant impact on this field, particularly in coordination with X-ray and radio observations.

**Acknowledgments:** We thank our collaborators Alice Harding, Apostolis Mastichiadis, Don Ellison, Steve Reynolds and Isabelle Grenier for many informative discussions about supernova remnants and shock acceleration theory. We also thank Joe Esposito for providing the images used in Figure 4.

## REFERENCES

1. Allen, G. E. et al. 1997, *Astrophys. J.* in press.
2. Arendt, R. G. 1989, *Astrophys. J. Supp.* **70**, 181.
3. Aschenbach, B., & Brinkmann, W. 1975, *Astron. Astr.* **41**, 147.

4. Baring, M. G. 1997 in *Proc. Les Arcs Moriond Workshop*, in press (2 reviews).
5. Baring, M. G., Ellison, D. C. & Grenier, I. A., in *The Transparent Universe*, eds. Winkler, C. et al. (ESA, SP-382, ESA, Noordwijk) p. 81.
6. Baring, M. G., et al. 1997, in these Proceedings.
7. Bartlett, L. M. 1994, Ph.D. Thesis, University of Maryland, unpublished.
8. Becker, W., Brazier, K. T. S. & Trümper, J. 1995, *Astron. Astr.* **298**, 528.
9. Blandford, R. D. & Cowie, L. L. 1982, *Astrophys. J.* **260**, 625.
10. Blandford, R. D. & Eichler, D. 1987, *Phys. Reports* **154**, 1.
11. Bork, T. 1989, Ph.D. Thesis, Ludwig-Maximilians-Universität, unpublished.
12. Borkowski, K. J. et al. 1996, *Astrophys. J.* **466**, 866.
13. Brazier, K. T. S., et al., 1996, *MNRAS* **281**, 1033.
14. Brazier, K. T. S., et al., 1997, *MNRAS* submitted.
15. Buckley, J. H., et al., 1997, *Astron. Astr.* in press.
16. Carter-Lewis, D. A., et al. 1997, Proc. 25th Int. Cosmic Ray Conf. (Durban), **3**, 161.
17. Chevalier, R. A. 1977, *Astrophys. J.* **213**, 52.
18. de Jager, O. C., & Harding, A. K. 1992, *Astrophys. J.* **396**, 161.
19. de Jager, O. C., et al. 1996a, *Astrophys. J.* **457**, 253.
20. de Jager, O. C., Harding, A. K., Sreekumar, P., & Strickman, M. 1996, *Astron. Astrophys. Suppl. Ser.* **120**, C441.
21. de Jager, O. C., Harding, A. K., & Strickman, M. 1996, *Astrophys. J.* **460**, 729.
22. de Jager, O. C., & Mastichiadis, A. *Astrophys. J.* **482**, 874.
23. Dermer, C. D. 1986, *Astron. Astr.* **157**, 223.
24. Dickel, J. R., Dickel, H. R., & Crutcher, R. M. 1976, *Pub. Astron. Soc. Pacific* **88**, 840.
25. Drury, L. O'C. 1983, *Rep. Prog. Phys.* **46**, 973.
26. Drury, L. O'C., Duffy, P. & Kirk, J. G. 1996, *Astron. Astr.* **309**, 1002.
27. Drury, L. O'C., Aharonian, F. A. & Völk, H. J. 1994, *Astron. Astr.* **287**, 959.
28. Drury, L. O'C., & Völk, H. J. 1981, *Astrophys. J.* **248**, 344.
29. Eichler, D. 1984, *Astrophys. J.* **277**, 429.
30. Ellison, D. C., Baring, M. G., & Jones, F. C. 1996, *Astrophys. J.* **473**, 1029.
31. Ellison, D. C., & Eichler, D. 1984, *Astrophys. J.* **286**, 691.
32. Ellison, D. C., & Reynolds, S. P. 1991, *Astrophys. J.* **382**, 242.
33. Ellison, D. C. et al. 1994, *Pub. Astron. Soc. Pacific* **106**, 780.
34. Esposito, J. A., et al., 1996, *Astrophys. J.* **461**, 820.
35. Frail, D. A., Goss, W. M., & Whiteoak, J. B. Z. 1994, *Astrophys. J.* **437**, 781.
36. Frail, D. A. et al. 1996, *Astrophys. J.* **464**, L165.
37. Gaisser, T. K., Protheroe, R. J. & Stanev, T. 1997, *Astrophys. J.* in press.
38. Giacalone, J., et al., 1993, *Astrophys. J.* **402**, 550.
39. Gould, R. J. 1965, *Phys. Rev. Lett.*, **15**, 577.
40. Green, D., SNR catalogue, <http://www.mrao.cam.ac.uk/surveys/snrs/>
41. Harding, A.K., de Jager, O.C., & Gotthelf, E. 1997, Proc. 25th Int. Cosmic Ray Conf. (Durban), **3**, 325.
42. Harrus, I. M., Hughes, J. P., Helfand, D. J. 1996, *Astrophys. J.* **464**, L161.

43. Hester J. J., et al. 1995, *Astrophys. J.* **448**, 240.
44. Higdon, J. C. & Lingenfelter, R. E. 1975, *Astrophys. J. (Lett.)* **198**, L17.
45. Hunter, S. D., et al. 1997, *Astrophys. J.* **481**, 205.
46. Hunter, S. D., Kinzer, R. L., & Strong, A. W. 1997, in these Proceedings.
47. Jones, F. C. & Ellison, D. C. 1991, *Space Sci. Rev.* **58**, 259.
48. Jones, L. R., Smith, A., & Angellini, L. 1993, *MNRAS* **265**, 631.
49. Jung, G. V. 1989, *Astrophys. J.* **338**, 972.
50. Kaaret, P. & Cottam, J. 1996, *Astrophys. J. (Lett.)* **462**, L35.
51. Kennel, C. F. & Coroniti, F. V. 1984, *Astrophys. J.* **283**, 694.
52. Keohane, J. W., Rudnick, L. & Anderson, M. A. 1996, *Astrophys. J.* **466**, 309.
53. Keohane, J. W., et al. 1997, *Astrophys. J.* **484**, 350.
54. Kifune, T. et al. 1995, *Astrophys. J.* **438**, L91.
55. Kifune, T. et al. 1997, to appear in *Towards a Major Atmospheric Čerenkov Detector*, ed. O. C. de Jager (Wesprint, Pochefstroom).
56. Koyama, K. et al. 1995, *Nature* **378**, 255.
57. Lagage, P. O. & Cesarsky, C. J. 1983, *Astron. Astr.* **125**, 249.
58. Lessard, R. W., et al. 1995, Proc. 24th Int. Cosmic Ray Conf. (Rome), **2**, 475.
59. Mastichiadis, A. & de Jager, O. C. 1996, *Astron. Astr.* **311**, L5.
60. Mastichiadis, A. 1996, *Astron. Astr.* **305**, L53.
61. Much, R. P., et al. 1995, *Astron. Astr.* **299**, 435.
62. Much, R. P., et al. 1996, *Astron. Astrophys. Suppl. Ser.* **120**, C703.
63. Müller, D., et al. 1995, *Proc. 24th ICRC (Rome)* **III**, 13.
64. Mukherjee, R., Grenier, I. A., & Thompson, D. J. 1997, in these Proceedings.
65. Naito, T. & Takahara, F. 1994 *J. Phys. G: Nucl. Part. Phys.* **20**, 477.
66. Pelling, R. M. et al. 1987, *Astrophys. J.* **319**, 416.
67. Pollock, A. M. T. 1985, *Astron. Astr.* **150**, 339.
68. Reynolds, S. P. 1996, *Astrophys. J. (Lett.)* **459**, L13.
69. Rho, J. et al. 1994, *Astrophys. J.* **430**, 757.
70. Sakurazawa, K. 1997, Proc. 25th Int. Cosmic Ray Conf. (Durban), **3**, 165.
71. Seward, F. D. 1989, *Space Sci. Rev.* **49**, 385.
72. Stecker, F. W. *Cosmic Gamma Rays*, (NASA SP-249, NASA, 1971)
73. Stephens, B. A., & Badhwar, G. D. 1981, *Astrophys. Sp. Sci.* **76**, 213.
74. Strickman, M., de Jager, O. C., & Harding, A. K. 1996, *Astron. Astrophys. Suppl. Ser.* **120**, C449.
75. Sturmer, S. J. & Dermer, C. D. 1995, *Astron. Astr.* **293**, L17.
76. Sturmer, S. J., et al., 1997, *Astrophys. J.* in press.
77. Tan, L. C. & Ng, L. K. 1983, *J. Phys. G: Nucl. Part. Phys.* **9**, 1289.
78. Tanimori, T., et al. 1997, IAU Circ. 6706.
79. Thompson, D. J. et al. 1994, *Astrophys. J.* **436**, 229.
80. Thompson, D. J. et al. 1996, *Astrophys. J. Suppl.* **465**, 385.
81. Vacanti, G., et al. 1991, *Astrophys. J.* **377**, 467.
82. Weekes, T. C. et al. 1989, *Astrophys. J.* **342**, 379.
83. Willmore A. P., et al., 1992, *MNRAS* **254**, 139.
84. Wootten, H. A. 1977, *Astrophys. J.* **216**, 440.
85. Yoshikoshi, T. 1996, Ph.D. Thesis, Univ. of Tokyo, unpublished.